Chemical Engineering Journal 501 (2024) 157557

Contents lists available at ScienceDirect

Chemical Engineering Journal

journal homepage: www.elsevier.com/locate/cej

Performance evaluation of resin wafer electrodeionization for enhanced nitrogen recovery from ammonium-containing water environment

Redae Nuguse Berhe [a,b], Yu-I Lin [c], Shu-Yuan Pan [c,d], Min Zhan [a], Hyunook Kim [a,*]

[a] Water-Energy Nexus Laboratory, Department of Environmental Engineering, University of Seoul, Seoul 02504, Korea
[b] Department of Chemical and Environmental Engineering, Ethiopian Institute of Technology, Mekelle 0231, Ethiopia
[c] Department of Bioenvironmental Systems Engineering, College of Bioresource and Agriculture, National Taiwan University, No. 1, Section 4, Roosevelt Road, Taipei City 10617, Taiwan ROC
[d] Agricultural Net-Zero Carbon Technology and Management Innovation Research Center, College of Bioresource and Agriculture, National Taiwan University, Taipei City 10617, Taiwan ROC

ARTICLE INFO

Keywords:
Ammonia-containing water
Ammonia removal
Continuous operation
Current efficiency
Electrodeionization
Resin wafer

ABSTRACT

Ammonium ion (NH_4^+) is a common pollutant from various sources like human and animal waste, industrial effluents, agricultural runoff, and commercial products, with traditional treatment methods often generating secondary contaminants, such as nitrite and nitrate. In this study, an energy-efficient resin-wafer electrodeionization (RW-EDI) process was employed for nitrogen recovery from ammonium-rich water. The system was operated in a continuous mode, with voltage-current curve measurements identifying a limiting current density of 2.2 A cm^{-2}. With the NH_4^+ concentration of 1 g/L and a flow rate of 2.4 mL min^{-1}, the system was tested at various cell voltages (1.2–7.2 V). The system could achieve 80 % NH_4^+ removal efficiency at a cell voltage of 3 V, current density of 2.2 A cm^{-2}, influent NH_4^+ level of 3 g/L, and flow rate of 6.4 mL min^{-1}. The observed current efficiency and the calculated power consumption were 41 % and 0.78 kWh m^{-3}, respectively. Finally, a mass balance model was developed to predict the number of RW-EDI stacks for complete removal of NH_4^+ from the feed. Overall, the result from this study demonstrates that the RW-EDI-based system could be a promising technology for recovering nitrogen from wastewater.

1. Introduction

Wastewater contains significant levels of ammonium (NH_4^+) ion, primarily due to the human and animal waste, household and industrial discharges, agricultural runoff, and commercial products [1–3]. The rapid growth of the fertilizer, food, and chemical industries has exacerbated the presence of these pollutants, making NH_4^+ among the most common water contaminant in agriculture and industrial wastewater [3,4]. Typically, domestic wastewater accounted for 60 to 70 % NH_4^+ and 30 to 40 % organic nitrogen, with concentration ranging from 20 to 100 mg/L [1,5,6]. After treating to some degree, most industries discharge their wastewater directly into surface waters, contributing high levels of NH_3 and NH_4^+, sulfate ions (SO_4^{2-}), chemical oxygen demand (COD), total organic carbon (TOC), and total alkalinity [1,6]. If released inappropriately treated, this wastewater can lead to eutrophication and harm aquatic life [7,8]. Therefore, it is essential treating both industrial and domestic wastewater to an acceptable level in an efficient and cost-effective manner.

Various methods for removing or recovering nitrogen from wastewater, such as stripping [1,4], chemical precipitation [9], absorption [10], reverse osmosis [11], and electrodialysis [2], have been employed [12,13]. However, these conventional technologies could produce secondary contaminants and require capital investment, limiting their industrial application [3,6]. In most cases, these physicochemical processes are combined with an activated sludge process for nitrification [14]. Nitrification, a two-step biological process, converts NH_4^+ into less harmful nitrites (NO_2^-) and nitrates (NO_3^-) [3,15]. Before discharging treated wastewater, denitrification may be necessary to reduce NO_3^- levels, but this process can contribute to sludge generation, posing additional management challenges [15]. Furthermore, the effectiveness of these processes can be influenced by dissolved oxygen (DO) levels, prolonged startup times, and slow microbial growth rate [16]. Therefore, integrating these multi-step processes with an efficient, cost-effective, and environmentally friendly technology is crucial for effective wastewater treatment.

* Corresponding author.
E-mail address: h_kim@uos.ac.kr (H. Kim).

https://doi.org/10.1016/j.cej.2024.157557
Received 7 July 2024; Received in revised form 28 October 2024; Accepted 8 November 2024
Available online 9 November 2024

Nomenclature

Acronyms

AMX	Anion-exchange
BP	bipolar
C_1-C_8	Concentrated samples collected from CACT
CACT	Captured NH_4^+ collecting tank
CE	Current efficiency
CMX	Cation exchange membrane
COD	Chemical oxygen demand
DO	Dissolved oxygen
ED	Electrodialysis
IEX	Ion exchange
PC	Power consumption
PFA444	Polystyrene Gel Type I Strong Base Anion Resin
PFC100E	Polystyrene Gel Strong Acid Cation Ion Exchange Resin
RO	Reverse osmosis
RW-EDI	Resin wafer electrodeionization
T_1-T_8	Treated samples collected from TACWCT
TACWCT	Treated NH_4^+-containing water collecting tank
TOC	Total organic carbon

Electrochemical oxidation has emerged as a promising method for removing of NH_4^+ from wastewater [17]. This technology offers operational simplicity, reduced sludge generation, and environmentally friendliness. However, it is energy-intensive and limited in application by product selectivity, pH control, system stability, and scalability issues [16,18]. In addition to electrochemical oxidation, electrodialysis (ED) is another process utilized for recovering NH_4^+ from wastewater. It is an electrochemical separation process that integrates dialysis and electrolysis, employing alternating ion exchange membranes between anode and cathode. As the solution resistance increases, the energy consumption of ED rises, leading to diminished recovery efficiency of NH_4^+. By utilizing a cation exchange membrane (CMX), NH_4^+ could be deprotonated to NH_3 gas on the cathodic surface and selectively stripped via the gas-permeable membrane. This process is most effective in recovering NH_3 from wastewater with a high NH_4^+ concentration (typically above 1 g-N L^{-1}) [2,19]. However, ED is less effective in recovering NH_3 and NH_4^+ from wastewater with a concentration less than 1 g-N L^{-1} due to concentration polarization.

Recently, electro-deionization (EDI) has emerged as a more efficient alternative to ED, offering lower electricity consumption, higher efficiency, improved product selectivity, and reduced resistance [20] and providing an advantage in dealing with concentration polarization of NH_4^+. The EDI technology leverages an electric field and ionically active media, such as ion-exchange resin integrated with electrodialysis and elution channels for waste streams [21]. When an electric potential is applied across the electrodes, ion adsorption and transportation begin on the ion exchange resin and ion exchange (IEX) membranes. The EDI stack configuration resembles that of ED; however, the inner compartment of an EDI stack is filled with a mixed cation and anion exchange resin bed. The resin bed serves as an ionic conductive medium, significantly reducing concentration polarization which can hinder effective ion removal and recovery [22,23]. Additionally, the ion exchange resin wafer has been designed to enhance the ionic conductivity, overcoming the high resistance encountered in the inner compartment [24].

Within the EDI stack, the electrodes induce a potential gradient that facilitates ionic transport [25]. Furthermore, water dissociation into H^+ and OH^- can occur at the electrode surfaces and at the interface of the resin beads, enabling continuous electrochemical regeneration of the resin [26,27]. The ion-exchange resin wafer can be regenerated by passing a concentrated solution of acids or bases through the resin bed, depending on the absorbed ions. For cation exchange resin, concentrated solution of hydrochloric acid (HCl) can replace the adsorbed NH_4^+ ions by hydrogen ions (Eqn. (1). Similarly, a strong base, such as sodium hydroxide (NaOH) solution, is used to regenerate anion exchange resins by replacing absorbed anionic ions like Cl^- with hydroxide ions (OH^-) (Eqn. (2).

Table 1
Physical and chemical characteristics of the ion exchange membranes.

Types of membrane	AMX	CMX	BP
Functional type	Strongly basic anion exchange	Strongly acidic cation exchange	
Functional form	Cl^- type	Na^+ type	
Thickness (mm)	0.20–0.30	0.25–30	0.17–0.28
Tensile strength (MPa)	≥0.90	≥0.35	≥0.70
Ion exchange capacity (meq (dry gram membrane)$^{-1}$)	2.7	1.89	
Water splitting capacity (%)			>98
Water splitting voltage (V)			0.9–1.8
Resistivity (Ω-cm^2)	2.0–3.0	1.8–3.8	<3
Thermal stability (℃)	≤40	≤40	≤40
Water permeability (mL h^{-1} cm^{-2} MPa^{-1})	≤0.1	≤0.1	≤0.1
Ion transport number (%)	>98 %	>98 %	
Selective penetration (%)	≥98	≥97	
pH operating range	<10	1–14	1–14

$$R - NH_4^+ + HCl \rightarrow R - H + NH_4Cl \quad (1)$$

$$R - Cl^- + NaOH \rightarrow R - OH + NaCl \quad (2)$$

where R is a resin polymer, R-NH_4^+ represents cation exchange resin in its NH_4^+-saturated form, R-H represents cation exchange resin in its regenerated form, R- Cl^- represents anion exchange resin in its Cl^--saturated form, and R- OH represents anion exchange resin in its regenerated form.

The power consumption of a resin-wafer electrodeionization (RW-EDI) stack can vary significantly based on its operational conditions, such as its size, the concentration and flow rate of feed, desired water quality, and operation time. A primary drawback of RW-EDI is its continuous high power consumption, along with the necessity for membrane cleaning and maintenance, which contributes to increased operating costs. Generally, the reported power consumption for running an RW-EDI system varies wide; it ranges from 0.2 to 1.55 kWh m^{-3} [21,22,28]. Nonetheless, it is much smaller than that a reverse osmosis (RO) system, which typically ranges 3.5 to 4.5 kWh m^{-3} [29], so RW-EDI is a more energy-efficient process.

In this study, we evaluated the nitrogen recovery efficiency of RW-EDI under continuous feed operation; while a few studies with the RW-EDI have been reported, all of them have been carried out in a batch mode. From a practical point of view, the continuous-feeding mode is more appropriate in assessing resource recovery efficiency of the system. The effects of critical parameters in RW-EDI, including feed concentration, feed matrix, flow rate, applied cell voltage, and current density on the NH_4^+ removal or recovery efficiency were investigated. Additionally, we analyzed current efficiency and power consumption along with the approximate saturation time of the resin wafer bed. Finally, a straightforward mass balance model was developed to estimate the number of stacks required based on the performance efficiency of a single RW-EDI stack.

2. Materials and methods

2.1. Chemicals and Materials

All chemical reagents used in this study were of analytical grade. Ammonium chloride (NH_4Cl, > 99.5 %), Sodium sulphate (Na_2SO_4, > 99 %), NaOH (> 98 %) and HCl (37 %) were purchased from Sigma-Aldrich (Seoul, Korea). The cathode used was stainless steel (9.54 cm

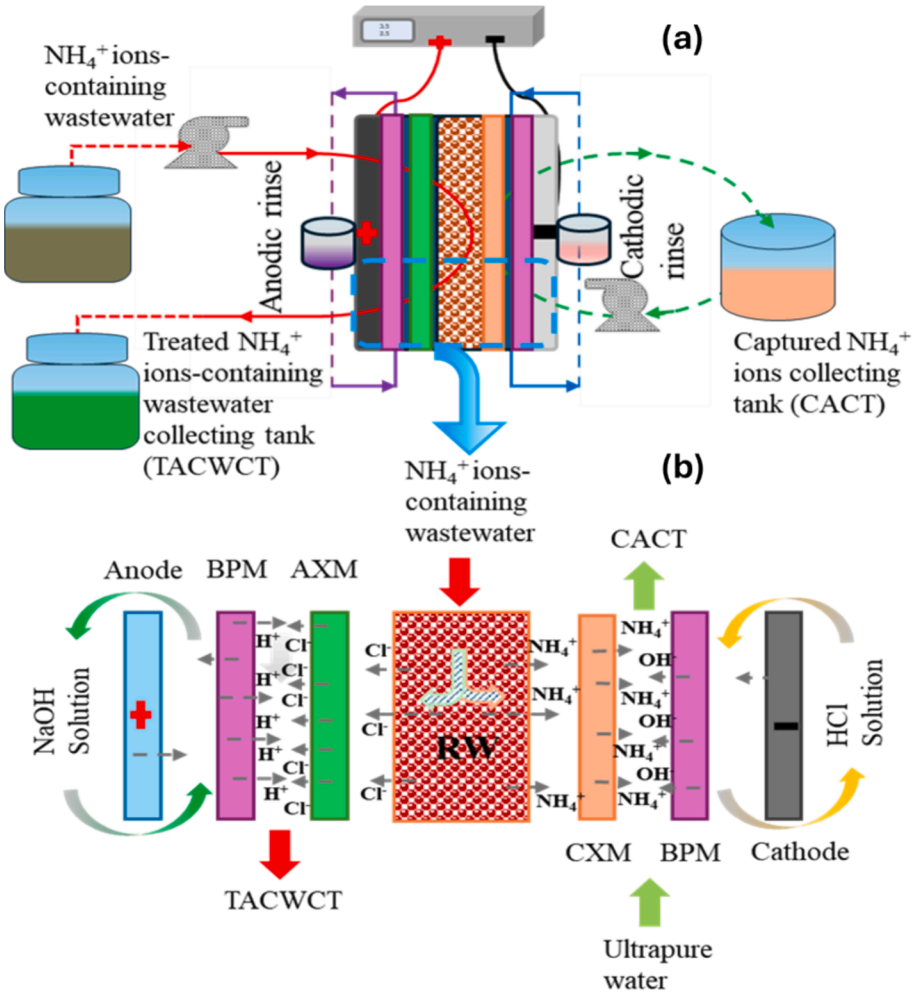

Fig. 1. The schematic representation of the overall RW-EDI system with all its components and flow-in and flow-out streams (a) and the internal configuration of the RW-EDI stack with its membrane arrangements (b).

× 4.6 cm × 0.16 cm), while the anode was composed of titanium dioxide (TiO_2) and ruthenium dioxide (RuO_2) sprayed stainless steel, with similar dimension to the cathode, were purchased from Sigma-Aldrich (Seoul, Korea). An EDI stack with 12 × 70 × 25 cm^3 dimension was provided by Ameridia Corp. (Somerset, NJ, USA). Commercially available cation-exchange (CMX), anion-exchange (AMX), and bipolar (BP) membranes having similar dimensions of 9.54 cm × 4.6 cm were purchased from Neosepta (Tokyo, Japan). Table 1 presents the physical and chemical characteristics of the membranes. Anion-exchange resin beads (Purofine PFA444) and cation-exchange resin beads (Purofine PFC100E) were purchased from Purolite LLC (Gyeonggi-do, Korea). A porous resin wafer bed was prepared by mixing of 1.3 g Purofine PFA444 and 1.3 g Purofine PFC100E and pressurizing at 120 ℃ [30]. The dimension of the resin bed was adjusted to 4.5 cm × 3.1 cm × 0.26 cm. High-purity water (resistivity higher than 18 MΩ cm at 25 ℃) was used to prepare solutions.

<Table 1>.

2.2. RW-EDI stack configuration

A lab-scale of NH_4^+-containing water recovery process based on a RW-EDI stack was conducted. Taking a specific characteristic directional movement of ions in the electric field into account, the ion exchange membranes were configured according to the target ions to be removed or recovered. Consequently, a BP was placed nearby the sides of both electrodes following gaskets. The anionic face of the BP was placed to the anode surface and its cationic face was aligned to the cathode surface to prevent ion loss to the electrodes [31,32]. The BP was then followed by AMX at the side of the anode and CMX on the side of cathode to facilitate anions and cations transport, respectively.

Typically, the configuration of the RW-EDI stack was arranged in the following order: anode, BP, AMX, RW, CMX, BP and cathode. The overall graphical representation of the RW-EDI configuration is described in Fig. 1a, and the combined stack of the system is called a single cell RW-EDI module (Fig. 1b). In this setup, the primary function of the BP was to prevent the loss of anion and cation due to anodic oxidation and cathodic reduction, respectively. Moreover, the BP was employed for water dissociation which could enhance the resin wafer regeneration process smoothly. Polyethylene mesh spacers (approximately 1 mm thick) were placed between each membrane to create gaps that facilitate ion exchange and water flow.

During the system configuration, four compartment flow channels were considered. These flow channels were crucial to the RW-EDI design, allowing for the independent flow of different streams. In brief, the anode-BP, BP-AMX, CMX-BP and BP-cathode interface channels were assigned for anolyte rinse solution ($NaSO_4$), NH_4^+-containing wastewater inflow channel, NH_4^+ ion capture inflow channel (ultrapure water circulation), and catholyte rinse solution (HCl) flow circulation, respectively. The electrode rinse solutions were employed to prohibit corrosion and rust formation on the anode and cathode due to electrochemical oxidation. The BP ensured these solutions did not mix with treated NH_4^+-containing water and the ultrapure water. Since the

Table 2
Specification of the commercially available Purofine PFA444 beads.

Polymer Structure	Gel polystyrene crosslinked with divinylbenzene
Appearance	Spherical Beads
Functional Group	Quaternary Ammonium
Ionic Form	Cl^- form
Total Capacity (min.)	1.1 eq L^{-1} (24.0 Kg ft^{-3}) (Cl^- form)
Moisture Retention	50–60 % (Cl^- form)
Mean Diameter	570 ± 50 μm
Uniformity Coefficient (max.)	1.3
Reversible Swelling, Cl^- → OH^- (max.)	30 %
Specific Gravity	1.07
Shipping Weight (approx.)	660–700 g L^{-1} (41.2–43.8 lb ft^{-3})
Temperature Limit	100 °C (212.0 °F) (Cl^- form)
Temperature Limit	60 °C (140.0 °F) (OH^- form)

Table 3
Specification of the commercially available Purofine PFC100E beads.

Polymer Structure	Gel polystyrene crosslinked with divinylbenzene
Appearance	Spherical Beads
Functional Group	Sulfonic Acid
Ionic Form	Na^+ form
Total Capacity (min.)	1.9 eq L^{-1} (41.5 Kg ft^{-3}) (Na^+ form)
Moisture Retention	46–50 % (Na^+ form)
Mean Diameter	570 ± 50 μm
Uniformity Coefficient	1.1–1.2
Reversible Swelling, Na^+ → H^+ (max.)	10 %
Reversible Swelling, Ca^{2+} → Na^+ (max.)	8 %
Specific Gravity	1.27
Shipping Weight (approx.)	795–830 g L^{-1} (49.7–51.9 lb ft^{-3})
Temperature Limit	120 °C (248.0 °F)

electrode rinse channels were protected by BPs to prevent from mixing with other flow-in and flow-out solutions of the RW-EDI stack. Additionally, the design minimized cross-mixing between NH_4^+-containing feed and ultrapure water stream by adjusting the position of the spacers inside the stack and using alternate inflow and outlet channels [33]. The anode and cathode were connected to an external DC power supply (Toyotech, TDP-3010B, Seoul, Korea) to drive the ions movement based on the potential difference. The electric current was measured and recorded every 5 min using a dual measurement multimeter (GDM-8342, Good Willing Instrument, Seoul, Korea). A porous resin wafer bed with mass of 2.6 g, volume of 3.51 cm^3 and surface area of 13.5 cm^2 was placed inside the stack to enhance NH_4^+ ions exchange. The average void fraction (36.7 %) and void space of the bed (2.3 cm^3) were estimated using bulk density method according to Eqn. 1S and 2S, respectively [30].

2.3. Resin pretreatment

Originally, PFA444 and PFC100E beads were in chloride (PFA444-Cl) and sodium (PFC100E-Na) forms, which were inactive for ion exchange due to their high ion counterbalance, requiring pretreatment. Prior to the experiment, the resin wafer mixture (PFA444-Cl and PFC100E-Na) was pretreated with 5 % of NaOH and 7 % of HCl for 30 min. After pretreatment, the resin wafer was regenerated into its active forms: PFA444-OH and PFC100E-H. The chemical reactions were presented in Eqns. (3) and (4), and the ion replacement mechanism is illustrated in Fig. S1a and b. The specifications of the PFA444 and PFC100E are detailed in Table 2 and Table 3, respectively.

$$PFA444-Cl^- + NaOH \rightarrow PFA444-OH^- + NaCl \quad (3)$$

$$PFC100E-Na^+ + HCl \rightarrow PFC100E-H^+ + NaCl \quad (4)$$

where PFA444-Cl and PFC100E-Na represent the chloride- and sodium-containing forms, while PFA444-OH and PFC100E-H are the regenerated forms.

After a series of batchwise rinses with HCl and NaOH, the RW-EDI system was washed with DI water to remove air bubbles. A feed tank was filled with 500 mL of NH_4Cl solution, which was injected into the anodic side of the RW-EDI stack. Treated NH_4^+-containing water was collected in an NH_4^+-containing water collecting tank (TACWCT). On the other side, 200 mL of ultrapure water was fed to capture NH_4^+ removed from the feed, which were then transferred to the captured NH_4^+ collecting tank (CACT) for simplicity. Moreover, the RW-EDI was equipped with an anode rinse solution (i.e., 2.5 % Na_2SO_4 of 500 mL) and a cathode rinse solution (i.e., 5 % of HCl of 500 mL), both recirculated within their respective compartments (Fig. 1) [27]. At the beginning of the experiment, streams were pumped at flow rate of 2.4 mL min^{-1} using peristaltic pumps (Masterflex L/S, model 7518–00, Temecula, CA 92590, California, USA).

2.4. RW-EDI limiting current density

At the start of the experiment, the limiting current of the RW-EDI was determined by varying the applied cell voltage (1.2–7.2 V), while the initial NH_4^+ concentration and flow rate were kept at 1 g L^{-1}, and 2.4 mL min^{-1}, respectively. The limiting current density, which is the minimum current required for water dissociation, is a key parameter for RW-EDI operation. At the applied cell voltages (voltage-current curve), the NH_4^+ removal efficiency of the RW-EDI was evaluated.

2.5. Sample collection and data analysis

After determining the optimal voltage-current condition, the system was operated at an applied cell voltage of 3 V, a current density of 2.2 A cm^{-2}, a flow rate of 2.4 mL min^{-1}, and an initial NH_4^+ concentration of 1 g L^{-1}. A 500 mL of NH_4^+-containing simulated wastewater and 200 mL of ultrapure water was pumped through RW-EDI. Treated NH_4^+-containing water and captured NH_4^+-containing water were collected at TACWCT and CACT, respectively. The process was repeated eight times and 1 mL of treated samples (T_1-T_8) from TACWCT and (C_1-C_8) from CACT were collected after each complete operation.

The pH and conductivity metrics of each sample that have been collected from TACWCT and CACT were measured by portable pH meter (6plus pH meter, Eutech Instruments, Singapore, Singapore) and conductivity meter (Conductivity/TDS meter, AF.23310, Taipei, Taiwan), respectively. Besides, the ion-exchange chromatography system (ICS-90, Thermo Fisher Scientific, Carlsbad, CA 92008, California, USA) was used to quantify the NH_4^+ present in both TACWCT and CACT according to Fig. S2 of calibration curve. The NH_4^+ removal efficiency and recovery rate were determined by Eqns. (5) and (6), respectively [33].

$$NH_4^+ \text{removal}\,(\%) = \frac{NH_4^+ \text{ ions removed at each operation}}{NH_4^+ \text{ initial concentration}} \times 100 \quad (5)$$

$$NH_4^+ \text{recovery}\,(\%) = \sum_{n=1}^{n} \frac{NH_4^+ \text{ ions recovered at each cycle}}{NH_4^+ \text{ initial concentration}} \times 100 \quad (6)$$

2.6. Resin wafer saturation time

Saturation time refers to the time by which the resin wafer capacity in the RW-EDI system is exhausted, a key indicator of its operational efficiency. It was determined by treating an excess volume of the NH_4^+ concentration of 3 g L^{-1} at operating conditions of 6.4 mL min^{-1} flow rate, current density of 2.2 A cm^{-2} and applied cell voltage of 3 V. The excess volume of the NH_4^+-containing wastewater was pumped in a

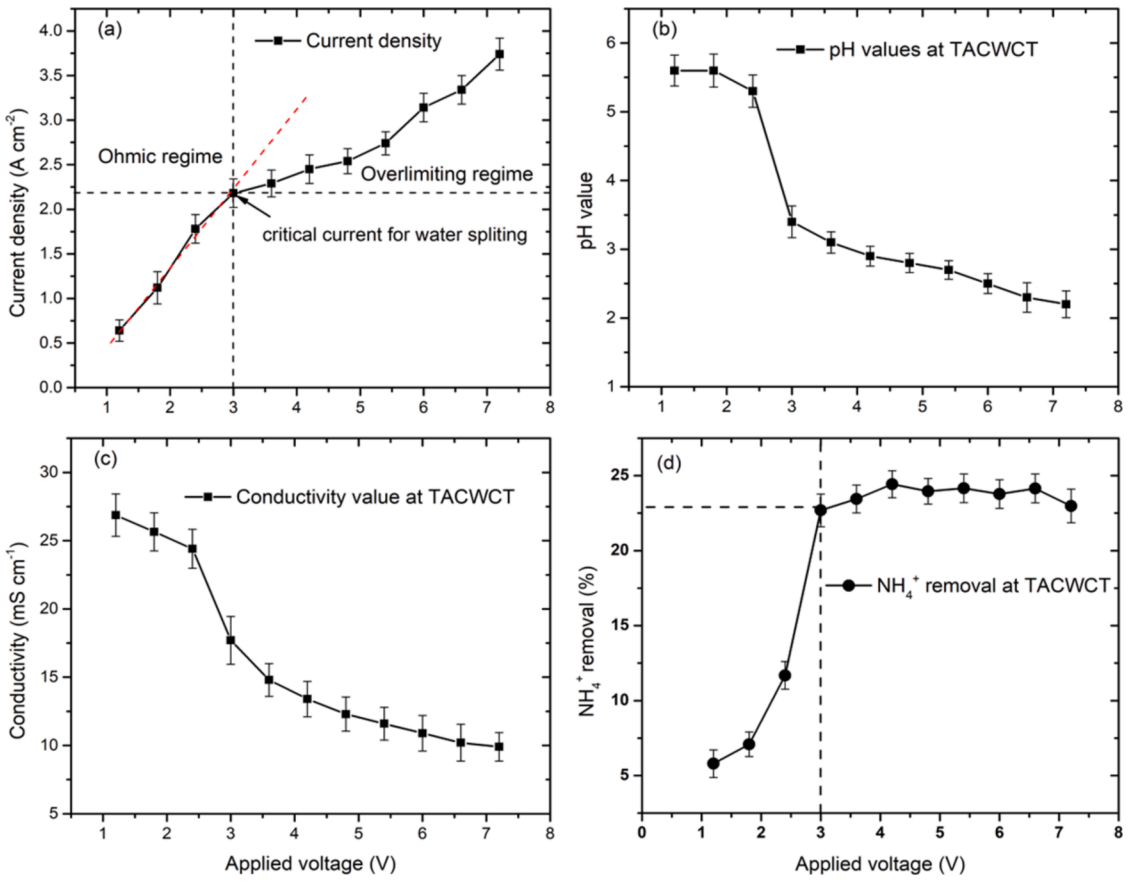

Fig. 2. The voltage-current curve to determine the limiting current and overlimiting current as function of applied voltage (a), pH variation at various applied voltage (b) conductivity change at various applied voltage (c) and NH_4^+ ions removal as a function of applied voltage (d) at constant initial NH_4^+ ions concentration of 1 g/L, flow rate of 2.4 mL min^{-1} and applied voltage of 1.2–7.2 V.

continuous mode (single pass) and collected into TACWCT. Whereas 200 mL ultrapure water was recycled through the cathodic side to capture NH_4^+ in CACT. Samples were collected every 10 min to monitor pH, conductivity, and concentration. The resin wafer was regenerated within 80–100 min of treatment time using HCl and NaOH.

2.7. Impact of operational parameters on RW-EDI performance

The impact of operational parameters on the RW-EDI performance was investigated at various flow rates (2.4, 4.4, 6.4, and 8.4 mL min^{-1}), applied cell voltage (1.3, 3.5, and 6.2 V) and initial NH_4^+ concentration (1, 3 and 5 g L^{-1}). NH_4^+ removal and recovery were measured by measuring NH_4^+ of the water samples collected from TACWCT and TACT. The amounts of NH_4^+ absorbed into the resin wafer were estimated according to Eqn. (7). After each experiment, the anodic and cathodic sides were rinsed with 5 % NaCl and 7 % HCl for 30 min followed by DI water to prevent membrane fouling.

$$\frac{\text{Mass of ions exchanged}}{\text{Mass of the resin}}\left(\frac{g}{g}\right) = \frac{\text{Total capacity}\left(\frac{eq}{L}\right) \times \text{Mw of } NH_4^+\left(\frac{g}{eq}\right)}{\text{Mass of the resin (g)}} \times \text{resin bed volume (L)} \tag{7}$$

where the mass of ions exchanged is NH_4^+ (g), total capacity is the capacity of the resin (eq), and the resin bed volume is the total volume of resin (L).

The NH_4^+ migration efficiency was linked to current efficiency (CE), calculated as the ratio of ion migration current to total current supplied. Determining the CE of the system provides an insight into the extent to which whether the NH_4^+ migration was being favored over side reactions such as excessive water dissociation at the given current supply [22,33]. CE and power consumption (PC) were estimated using Eqns. (8) and (9), respectively [34].

$$CE\,(\%) = \frac{zFV \times C_{NH_4^+\ \text{after treatment}}}{MW_{NH_4^+}\int_0^t Idt} \times 100 = 8.94 \times \frac{V \times C_{NH_4^+\ \text{after treatment}}}{I \times t} \tag{8}$$

$$P_c\left(kWh\,m^{-3}\right) = \frac{E_{cell} \times I \times t}{V_{NH_4^+}\ \text{treated}} = \frac{50}{3}\frac{E_{cell} \times I \times t}{V_{NH_4^+\ \text{treated}}} \tag{9}$$

where z is the valence of NH_4^+, F is the Faraday's constant (96,486C mol^{-1}), V (mL) is the volume of the NH_4^+-containing feed solution, C (g L^{-1}) is the concentration of NH_4^+ after treatment during the specified time of the RW-EDI operation, MW_{NH4}^+ (g mol^{-1}) is the molecular weight of NH_4^+ (18.04 g mol^{-1}), I (A) is the current applied to the RW-EDI stack, E_{cell} (V) is the applied cell voltage across the electrodes in the RW-EDI module, and t (min) is the time duration of the RW-EDI operation. For economic consideration, the feasibility of the process was assessed by estimating its overall cost-effectiveness.

Lastly, a material balance model between the RW-EDI stack [34] was set up to predict the number of RW-EDI stacks required for complete NH_4^+ removal at an initial NH_4^+ concentration of 3 g L^{-1}, flow rate of 6.4 mL min^{-1}, current density of 2.2 A cm^{-2}, and applied cell voltage of 3 V. Finally, the model was correlated to the NH_4^+ removal efficiency measured by a single RW-EDI stack.

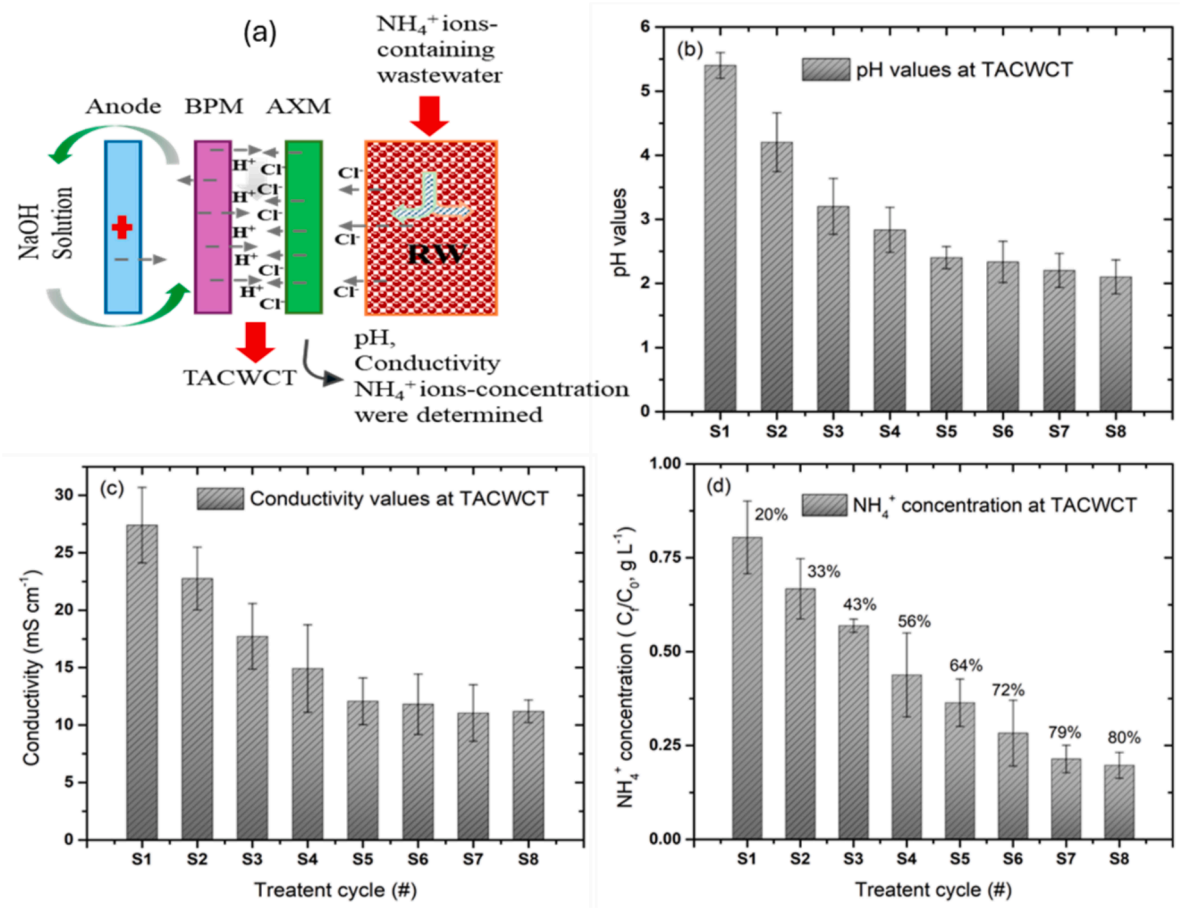

Fig. 3. Evaluation of the performance of the RW-EDI; half section of the RW-EDI which describes the treated NH_4^+ ions-containing water collecting tank (TACWCT) (a), pH variation as a function of number of treatment cycles (b), electrical conductivity variation along the treatment cycles (c) and NH_4^+ ions concentration variation (d) at a constant applied voltage of 3 V, current density of 2.2 A cm^{-2}, initial NH_4^+ ions concentration of 1 g/L and flow rate of 2.4 mL min^{-1}.

3. Results and Discussion

3.1. Limiting current and removal efficiency

Unlike simple electrochemical cells without a membrane, RW-EDI does not exhibit a horizontal plateau at the limiting current density. Instead, its voltage-current curve shows a gradual increase in slope to an over-limiting current regime [35]. Current saturation is not reached because the system lacks a clear limiting current, but a slope change at a critical current signal the onset of water dissociation. This overlimiting current is caused by the loss of permeable selectivity of the membranes for H^+ and OH^- due to water dissociation. Since the plateau indicating the limiting current was not observed, the critical current was identified by extrapolating the linear line of voltage-current curve of Ohm's law [35,36]. The critical current density of the system was determined by increasing the voltage across the RW-EDI stack and at the same time measuring the corresponding current at which water dissociation occurs. This critical current signal serves as a reference for further experiment. [26].

As shown in Fig. 2a, the voltage-current curve was analyzed in two regimes. At lower voltages (1.2–3 V), Ohm's law was applied with roughly constant resistance, likely due to minimal NH_4^+ depletion and concentration polarization nearby membranes or resin. As concentration polarization develops due to the depletion of NH_4^+ in the bulk solution, the electrical resistance increased with the applied cell voltage [37]. The reduced NH_4^+ concentration near the membrane and resin surface made fewer ions available to carry the current, increasing resistance, particularly at a higher voltage. This concentration polarization reduced NH_4^+ availability, further raising electrical resistance of the system. During the experiment, a slope change without a clear plateau was observed at a current density of 2.2 A cm^{-2} and 3 V, indicating a drop in NH_4^+ concentration near to the membranes. This specific point of current and applied cell voltage were considered as the minimum voltage-current curve for water dissociation in this RW-EDI system. As the applied voltage exceeded further to 6 V, another slope change was observed, which should indicate the over-limiting current regime. The slope of the line in this regime was lower than the one in the Ohmic region. Thus, the minimum voltage for water dissociation was near 3 V, significantly higher than the ideal water dissociation voltage of 1.23 V [38]. The pH drop observed at 3 V should be due to H^+ generation from water dissociation (Fig. 2b). Since the water dissociation voltage is crucial for the continuous resin regeneration, this minimum voltage at the critical current was determined. Similarly, a significant conductivity change was observed from 3 V and the critical current density of 2.2 A cm^{-2} (Fig. 2c).

To determine which voltage-current regime would be more effective in removing NH_4^+, the removal efficiency was calculated at each applied voltage (1.2–7.2 V). Higher efficiencies were observed in the over-limiting current regime (Fig. 2d). The removal efficiency of NH_4^+ improved dramatically as the voltage transitioned from the Ohmic to the overlimiting current regime. However, further increasing the voltage in the overlimiting regime did not improve the removal efficiency. The higher removal rate in this regime was attributed to the increased charge transfer and electroconvection [39]. The greater charge transfer was facilitated by the new current carriers, such as H^+ and OH^- generated via water dissociation at the NH_4^+ depleted membrane surfaces [40]. Thus,

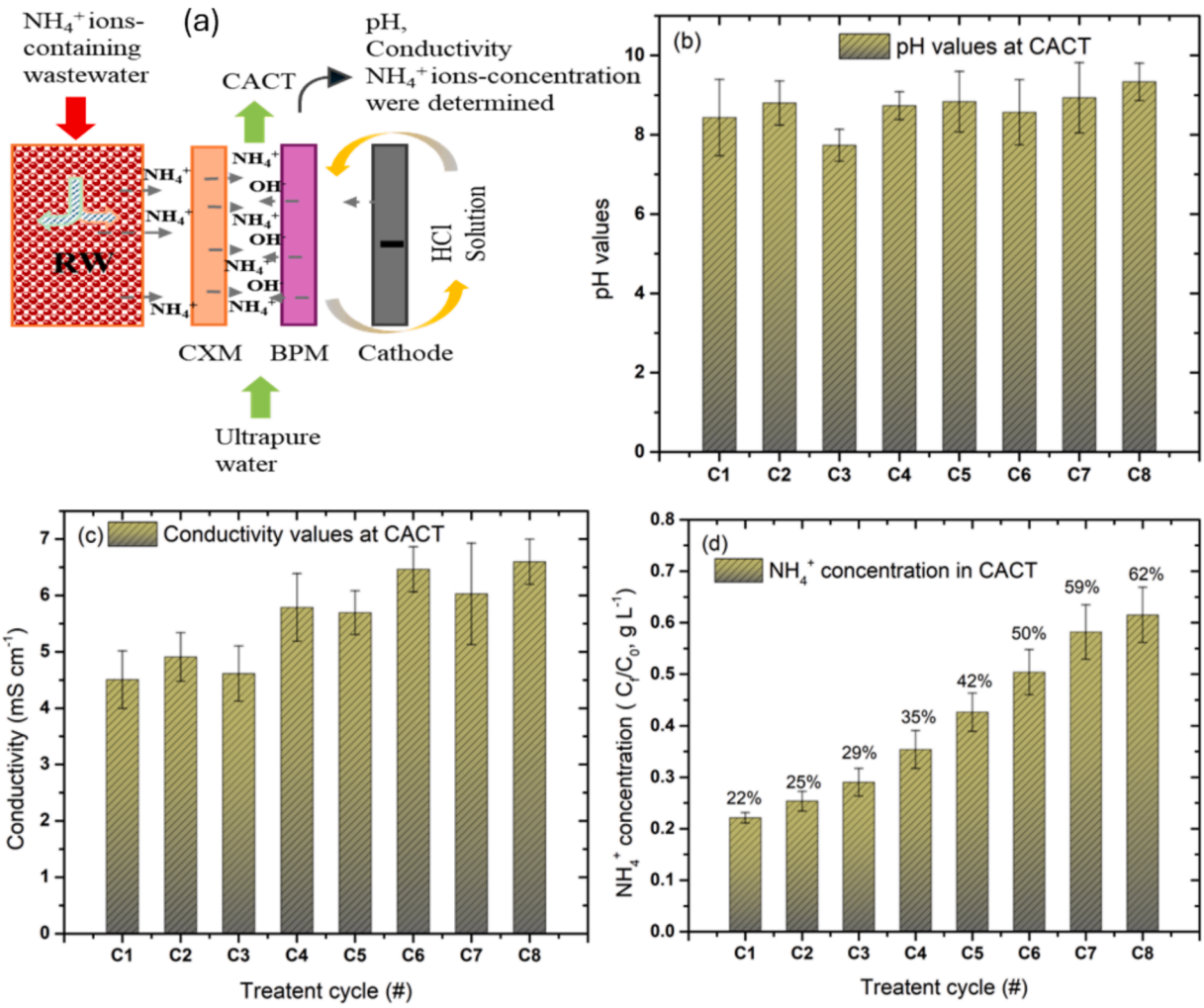

Fig. 4. Evaluation of the performance of the RW-EDI; half section of the RW-EDI which describes the captured NH_4^+ ions collecting tank (CACT) (a), pH variation as a function of number of treatment cycles (b), electrical conductivity variation along the treatment cycles (c) and NH_4^+ ions concentration variation (d) at a constant applied voltage of 3 V, current density of 2.2 A cm^{-2}, initial NH_4^+ ions concentration of 1 g/L and flow rate of 2.4 mL min^{-1}.

the overlimiting current regime was deemed as the optimal further RW-EDI operation. Liao et al [28] also obtained a higher CE (44 %) and a lower PC (0.78 kWh m^{-3}) at the critical current density of 2.2 A cm^{-2} and 3 V.

3.2. RW-EDI performance evaluation

Fig. 3 presents data generated by analyzing samples collected from the TACWCT. Changes in pH, conductivity, and NH_4^+ concentration would provide insights into the RW-EDI stack configuration, experimental setup, and performance efficiency. Fig. 3a illustrates how treated NH_4^+-containing water was collected through the junction of membrane channels, specifically at the BP-AMX intersection. This surface interaction forces the water through the membrane junction into the TACWCT.

Fig. 3b depicts the pH change as a function of treatment cycles. As seen from Fig. 3b, increasing the number of treatment cycles could result in the pH drops of the treated NH_4^+-containing water. As mentioned earlier, the RW-EDI was operated near the over-limiting current regime, where water dissociation occurred at the BP-AMX and resin bead junctions. This regime was characterized by a comparatively high voltage and high current density. The generated H^+ can combine with Cl^-, leading to HCl generation, which would explain the pH drop in the TACWCT. Another possibility is the selective transport of H^+ generated by water dissociation along with the treated NH_4^+-containing water through the membrane channels.

Water dissociation causes dynamic concentration changes near the ion exchange membranes and resins . Since H^+ diffuses much faster than Cl^-, this contributes to the pH drop in TACWCT. Several studies have reported similar pH changes in EDI systems, with the pH of solutions pumped to the dilute compartment (the resin-resin channel) being higher than the influent solution [41–43].

Fig. 3c demonstrates electrical conductivity changes in TACWCT samples during treatment cycles. Like the pH data, the conductivity decreased over successive cycles, indicating continuous ion depletion. After the fifth cycle, no further conductivity change was observed, indicating that the resin wafer had reached its maximum ion exchange capacity. A similar observation was also reported by Zhao et al. [41]. The decrease of conductivity was further supported by the NH_4^+ dynamics as a function of treatment cycles. As shown in Fig. 3d, the NH_4^+ concentration gradually decreased over the cycles, with the RW-EDI system achieving removal efficiency of 80.3 % after the eighth cycle. After the seventh cycle, the performance efficiency of the RW-EDI stack became lower. The treatment cycles were modeled as if eight RW-EDI stacks of equal efficiency were connected in series. It was noted that some of NH_4^+ in the feed was pumped out to TACWCT, some adsorbed by the resin wafer, some vaporized as NH_3 gas, and some recovered into CACT.

Similarly, samples from CACT were analyzed, with the results shown

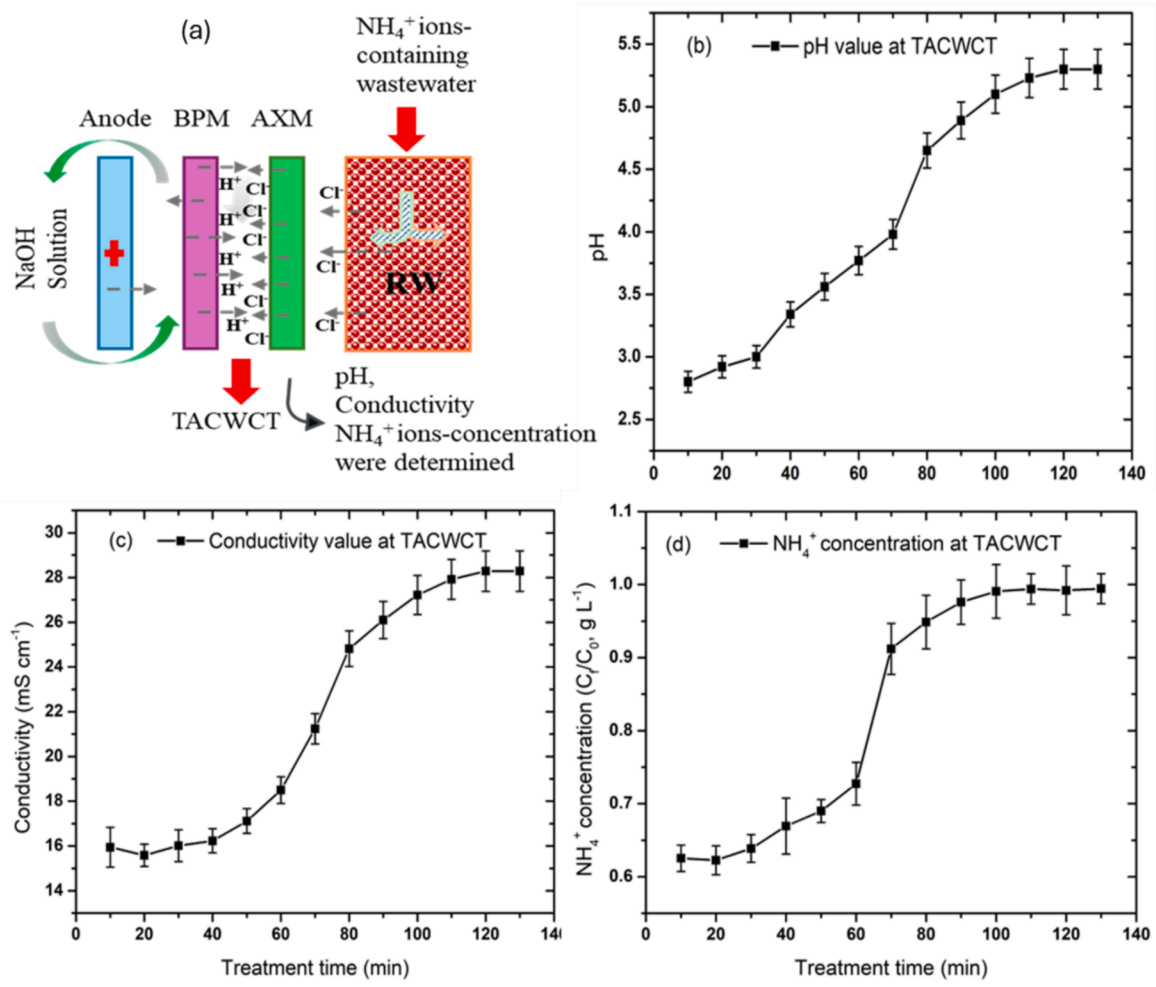

Fig. 5. Determination of saturation time of the resin wafer; half section of the RW-EDI which describes the treated NH_4^+ ions-containing water collecting tank (TACWCT) (a), pH variation as a function of treatment time (b), electrical conductivity variation along the treatment time (c) and NH_4^+ ions concentration variation as a function treatment time (d) at a constant applied voltage of 3 V, current density of 2.2 A cm^{-2}, and flow rate of 6.4 mL min^{-1}.

in Fig. 4. The captured NH_4^+ was analyzed over several cycles in terms of pH, conductivity, and NH_4^+ concentration change. Fig. 4a describes the NH_4^+ recovery by the CMX-BP channel connected to CACT, which was designed to allow only NH_4^+ to pass. Fig. 4b indicates the minimal pH fluctuations over the eight treatment cycles, with the pH stabilizing between 7.8 and 9.4, which was higher than the pH of the initial NH_4^+-containing water. The NH_4^+ collected through the CMX-BP channel was counter-balanced by the OH^- generated via water dissociation at the CMX-BP interface. As a result, NH_4^+ would form NH_4OH, raising the solution to a more alkaline environment.

Fig. 4c presents the electrical conductivity data of the CACT samples over eight cycles. An overall increase in conductivity was observed, with a final conductance of 7.12 mS cm^{-1} achieved over the eighth cycle. However, this increase was not linear, probably because the samples were repeatedly reinjected to the RW-EDI stack. The NH_4OH solution may have undergone dissociation phase to NH_4^+ and OH^-, contributing to the high conductivity. Additionally, NH_4^+ may have been dehydrogenated to ammonia (NH_3) gas, resulting in lowering the solution conductivity. Fig. 4d shows the cumulative NH_4^+ concentration of CACT over the treatment cycles, with NH_4^+ recovery increasing from cycle one (C_1) to cycle eight (C_8). By eight cycles, NH_4^+ of 61.5 % could be recovered via the CMX-BP channel into CACT, while 19.7 % of NH_4^+ in the feed had been pumped through the BP-AMX channel into TACWCT, and 18.8 % had been either lost as NH_3 or absorbed onto the resin surface.

3.3. Resin wafer saturation time

The saturation time of the resin wafer was thoroughly investigated by analyzing the pH, conductivity, and NH_4^+ concentration in TACWCT and CACT as a function of treatment time. As presented in Fig. 5, the performance of the RW-EDI system was assessed by varying different parameters (i.e., applied voltage, current density, flow rate, and initial NH_4^+ concentration). Fig. 5a presents the half section of the RW-EDI configuration; a linear increase in the pH was observed during the treatment: from 2.8 to 5.4 (Fig. 5b). The pH increase was attributed to the gradual decrease of NH_4^+ over the treatment time. As the active functional groups of resin wafer reached periodic saturation, the NH_4^+-containing water was inadequately treated, potentially contributing to the pH rise in TACWCT [44]. Moreover, dynamic changes of ions at the membrane-membrane, membrane-resin, or resin-resin surface could have contributed to the pH increase [21]. After 100 min, the pH pattern approached a plateau, and no further pH change was observed.

The electrical conductivity of the samples followed a similar trend to the pH (Fig. 5c). During the first 80 min, a sigmoidal increase in conductivity was recorded. However, an approximate horizontal plateau was established after 80 min. Beyond this point, a significant change in the conductivity profile was not observed. Fig. 5d shows the NH_4^+ profile over the treatment period; the profile follows a sigmoidal curve in a similar manner to the other parameters. Over the first 60 min, the NH_4^+ concentration did not show much change. However, after 70 min, there was a sharp change, with the concentration of NH_4^+ in TACWAT nearly

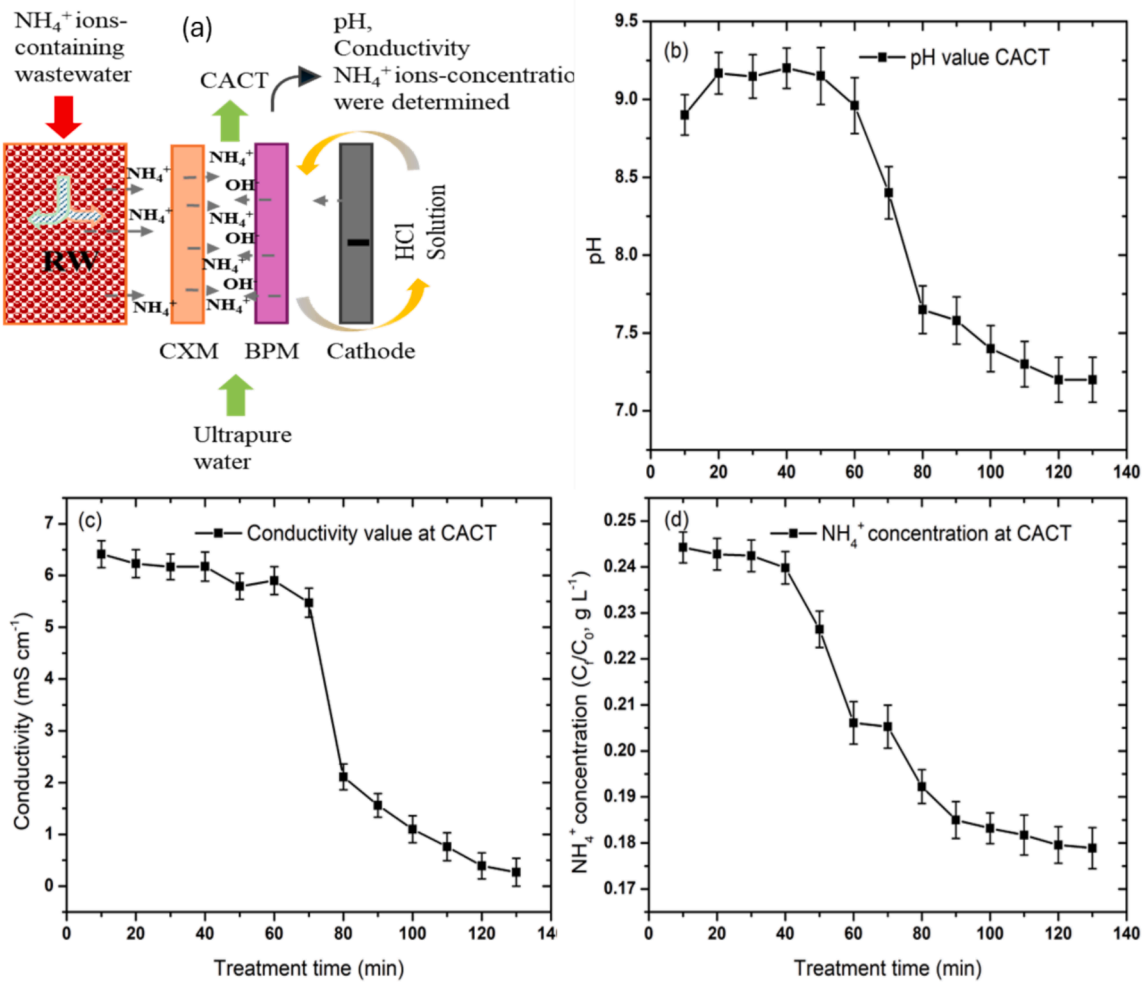

Fig. 6. Determination of saturation time of the resin wafer; half section of the RW-EDI which describes the captured NH_4^+ ions collecting tank (CACT) (a), pH variation as a function of treatment time (b), electrical conductivity variation along the treatment time (c) and NH_4^+ ions concentration variation as a function treatment time (d) at a constant applied voltage of 3 V, current density of 2.2 A cm^{-2}, and flow rate of 6.4 mL min^{-1}.

matching that of the influent. The NH_4^+ concentration achieved a horizontal plateau, suggesting the maximal capacity of the resin wafer. The horizontal plateau signaled the full saturation of the resin wafer; after the plateau was observed, the RW-EDI performance efficiency declined. Based on this, the saturation time was determined to be 100 min. So, the wafer resin was determined to regenerate 100 min after each continuous operation of the RW-EDI. The onset of the plateau in both pH and conductivity profiles is a critical moment for regenerating the resin wafer, and the same can be said for the NH_4^+ concentration plateau.

Similarly, the pH, conductivity, and NH_4^+ concentration of the CACT samples were analyzed. The NH_4^+ recovery track through CMX-BP channel compartment was coupled to CACT (Fig. 6a). This membrane junction is designed to allow the passage of NH_4^+ only. Insignificant pH (Fig. 6b) and conductivity (Fig. 6c) changes were observed over the first 70 min. However, after 80 min, the pH and conductivity values dramatically changed approximately from 9.2 to 7.1 and 6.3 to 0.7 mS cm^{-1}, respectively. Reaching minimum values for both pH and conductivity in CACT indicated the gradual exhaustion of the capacity of the resin wafer in NH_4^+ exchange. The NH_4^+ concentration profile, shown in Fig. 6d, followed a similar pattern. No significant changes were observed during the first 80 min, but after this point, NH_4^+ concentration dropped sharply, reaching negligible levels. Like the pH and conductivity, the NH_4^+ concentration reached a lower marked plateau, indicating the ion exchange capacity of the resin. This plateau marked the saturation of the resin wafer and reduced performance of the RW-EDI system. It was noted that the efficiency of the RW-EDI was lowered as the treatment time continued. It was worth noting that the beginning of pH, conductivity and NH_4^+ drop could be a crucial indicator for the resin regeneration. The establishment of the lower plateau further suggests the optimal time for resin regeneration. Therefore, while treating 3 g L^{-1} NH_4^+ at the working voltage, current density, and flow rate of 3 V, 2.2 A cm^{-2} and 6.4 mL min^{-1}, respectively, the RW-EDI was required to regenerate at every 100 min of operation. On the other hand, the resin regeneration was required after treating 6.4 L of NH_4^+-containing water under the mentioned operating parameters.

3.4. *Effect of operational parameters on RW-EDI performance*

As shown in Fig. 7, the effects of operational parameters such as flow rate, applied cell voltage, and initial NH_4^+ concentration on the RW-EDI performance were investigated. Different flow rates (2.4, 4.4, 6.4, and 8.4mL min^{-1}) were tested with corresponding residence times of 91, 50, 34, and 26 s, respectively. The RW-EDI performance was evaluated at a voltage of 3 V, a current density of 2.2 A cm^{-2}, and an initial NH_4^+ concentration of 1 g L^{-1}. Fig. 7a and b show that NH_4^+ removal occurred faster at lower flow rates, with the resin bed saturating more quickly. For example, at 4.4 mL min^{-1}, the RW-EDI performance declined after treating 180 mL of NH_4^+-containing water within 40 min. Increasing the flow rate from 6.4 to 8.4 mL min^{-1} extended the RW-EDI operation time before a regeneration from 70 min to100 min, eventually treating 450

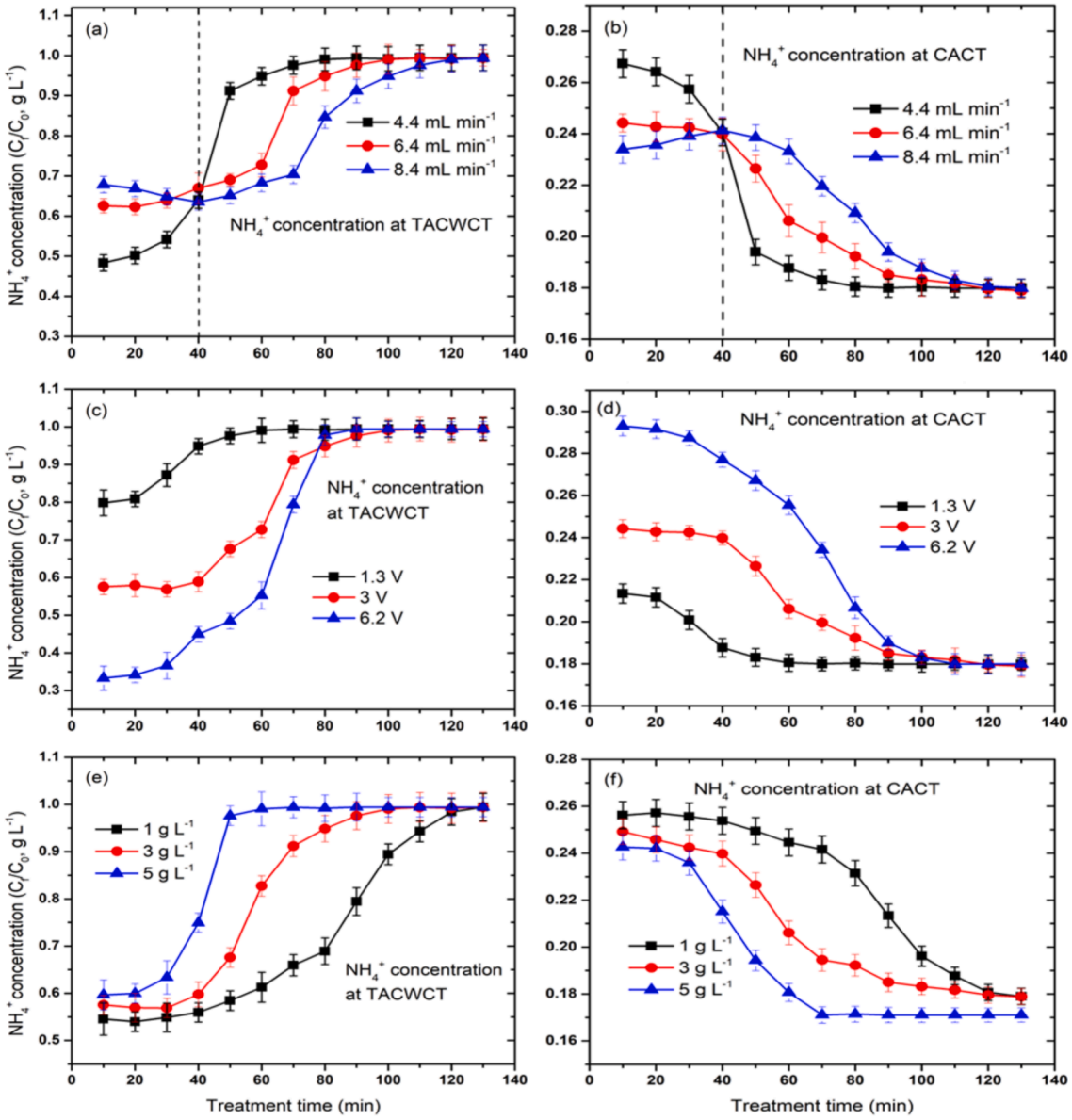

Fig. 7. The effect of operational parameters on the NH_4^+ removal efficiency at TACWCT and the NH_4^+ recovery efficiency at CACT: The effect of flow rate on NH_4^+ removal (a) and NH_4^+ recovery (b), the effect of cell voltage on NH_4^+ removal (c) and NH_4^+ recovery (d), and the effect of initial concentration on NH_4^+ removal (e) and NH_4^+ recovery (f).

mL and 840 mL of water, respectively. However, lower flow rates resulted in a higher NH_4^+ removal efficiency before resin saturation; removal efficiencies of 47 %, 33 %, and 27 % were achieved at the flow rates of 4.4, 6.4, and 8.4 mL min^{-1}, respectively [25].

Similar results were reported by Rathi & Kumar [27], who observed a higher As removal efficiency at lower flow rates. Contrarily, Sarıçiçek *et al.* [24] observed higher removal at high flow rates, and Pan et *al.* [22] demonstrated minor effect of flow rates on RW-EDI performance. In a continuous feed mode, lower flow rates indicate a longer residence time, increasing a better ion exchange efficiency. After 40 min of treatment, all flow rates showed similar NH_4^+ removal efficiency, a critical point where flow rate became irrelevant to performance (Fig. 7a). The same trend was observed for CACT over 100 min of treatment time (Fig. 7b). A shorter operation time at a lower flow rate was due to slower NH_4^+ movement through the resin wafer, allowing more time for adsorption [45]. At higher flow rates, faster NH_4^+ exchange occurred, though contact time was reduced. Table 4 presents a comparison of the RW-EDI system performance using various ion exchange resins.

Fig. 7c and d illustrate the effects of various applied cell voltages (i. e., 1.3, 3 and 6.2 V) on RW-EDI performance. Increasing voltage improved NH_4^+ removal rates, with maximum efficiencies of 19 %, 39 %, and 47 % at 1.3, 3, and 6.2 V, respectively, within 20 min. However, after 80 min, further voltage increases had no effect, as resin saturation was reached. Higher voltages also increased NH_4^+ recovery at CATC, with 21 %, 25 % and 29 % recovered within the first 20 min at 1.3, 3 and 6.2 V, respectively. Beyond 80 min, NH_4^+ concentration changes flattened, suggesting water dissociation consumed additional voltage, affecting removal efficiency and altering pH and conductivity [32]. Excessive voltage also generated H^+ and OH^- ions, which helped regenerate the resin wafer but also participated in ion exchange, further boosting NH_4^+ removal [45].

The CE and PC were heavily influenced by voltage, as shown in Fig. S3. Raising the voltage from 1.3 V to 6.2 V increased NH_4^+ removal but also boosted power consumption, with a drop in CE [21,47]. A 3 V applied voltage was the best condition, removing 79 % of NH_4^+ over eight cycles, with a balance between CE (41 %) and PC and (0.76 kWh

Table 4
Comparison of RW-EDI Device Performance with Different Ion Exchange Resins.

EDI Parameters	This Work	Fasuyi & Lopez [33]	Zheng et al., [32]	Sun et al., [46]	Zhang & Chen [45]	Khoiruddin et al., [25]
Resin Type	Mixture of Purofine PFA444 and Purofine PFC100E	Mixture of Amberlite® IRA-400 and Amberlite® IR120	Mixture of Purofine PFA444 and Purofine PFC100E	Amberlite IRA 402 and Amberlite IR 120	Amberlite® IRA900RF and Amberlite® 200C	Amberlite IRA900 and Amberlite IRA120
Ion Exchange Mode	Anion and Cation	Anion and Cation	Anion and Cation	Anion and Cation	Anion and Cation	Anion and Cation
Removal Efficiency	80 %	90	83.3 %	88.2	90.7	83.4
Current Efficiency	41 %	–-	–-	–-	–-	–-
Power Consumption	0.78 $kWhm^{-3}$	2.25 $kWhm^{-3}$	0.66 $kWhm^{-3}$	–-	–-	33.3 $kWhm^{-3}$
Operating Voltage	3 V	8 V	2.28 V	150 V	2.7 V	50 V
Current Density	2.2 Acm^{-2}	0.225 Acm^{-2}	–-	0.3 Acm^{-2}	0.32 Acm^{-2}	0.12 Acm^{-2}
Flow Rate	24 $mLmin^{-1}$	–-	810 $mLmin^{-1}$	60 $mLmin^{-1}$	9 $mLmin^{-1}$	0.03 $mLmin^{-1}$
Resin Bed Volume	3.51 cm^3	3.125 cm^3	50.7 cm^3	40 cm^3	15.6 cm^3	37.4 cm^3
Resin Bed Surface Area	13.5 cm^2	12.5 cm^2	195 cm^2	200 cm^2	60 cm^2	144 cm^2
Applied in	Ammonium recovery	Desalination process	Desalination process	Purification process	Nitrate removal	Desalination process

m^{-3}). Higher voltage (6.2 V) raised PC to 1.6 kWh m^{-3} and reduced CE to 37 %, likely due to high water dissociation reaction. Operating at 3 V proved economically feasible, minimizing power use while maintaining high NH_4^+ removal efficiency, making this system a cost-effective approach for large-scale wastewater treatment.

The effect of initial NH_4^+ concentration on RW-EDI efficiency was also critical for predicting long-term performance. Higher initial concentrations lead to faster resin saturation, requiring more frequent regeneration and potentially higher applied voltages, which can increase PC. Experiment analysis was conducted with NH_4^+ concentrations of 1, 3 and 5 g L^{-1} (Fig. 7e and f), with no significant change in NH_4^+ removal efficiency at the start. Operating at 3 V, 2.2 A cm^{-2}, and a flow rate of 6.4 mL min^{-1}, the RW-EDI system performed best at lower concentrations (1 g L^{-1}), sustaining efficiency for over 120 min and treating 770 mL of water. After 120 min, NH_4^+ removal plateaued. At higher concentration (5 g L^{-1}), resin saturation occurred sooner, after treating 320 mL of water, due to higher NH_4^+ levels. At high concentration, higher adsorption capacity of the ions into the resin wafer with 23.6 mg g^{-1}, compared to 8.3 mg g^{-1} at 1 g L^{-1} NH_4^+ concentration, Similar to results reported by Yaragal and Mutnuri [48] for nitrate removal. The ratio of NH_4^+ concentration in effluent tank to the initial NH_4^+ concentration after resin saturation was observed to be higher than unity. The increase in the NH_4^+ concentration ratio was explained due to the disturbance and desorption of the NH_4^+ that have been previously absorbed. While the saturated resin wafer starts to release some of the adsorbed NH_4^+, causing an increase in the ratio of NH_4^+ concentration. Fig. 7f shows higher NH_4^+ concentration at CACT when lower initial NH_4^+ concentrations were used.

3.5. Resin regeneration

Resin saturation time is a critical operating parameter in the RW-EDI operation. It signals that the resin can no longer efficiently exchange NH_4^+, and regeneration is required. Specifically, PFC100E becomes saturated with NH_4^+, forming PFC100E-NH_4^+, and PFA444 becomes saturated with Cl^-, forming PFA444-Cl. The resin beads are then regenerated to their functional ion-exchange forms using a crossflow of 7 % HCl and 5 % NaOH through the resin bed. After 30 min, NH_4^+ in PFC100E-NH_4^+ is replaced by H^+ (Eqn. (10), and Cl^- in PFA444-Cl is replaced by OH^- (Eqn. (11). The resin regeneration process was carried out typically 100 min after a continuous operation of the RW-EDI system under the operating conditions of 3-g L^{-1} NH_4^+, 3-V applied voltage, 2.2-A cm^{-2} current density, and 6.4-mL min^{-1} flow rate. After regeneration, the RW-EDI regained its exchange capacity according to Fig. S4. On the other hand, the functional groups were assessed using FT-IR technique before and after regeneration as presented in Fig. S5.

$$PFC100E - NH4 + + HCl \rightarrow PFC100E - H^+ + NH4Cl \quad (10)$$

$$PFA444 - Cl^- + NaOH \rightarrow PFA444 - OH^- + NaCl \quad (11)$$

where PFC100E-NH_4^+ and PFC100E-H represent the saturated and regenerated forms of cationic resin while PFA444-Cl and PFA444-OH represent the saturated form and regenerated forms of anionic resin.

3.6. Mass balance based module predictive model

Making a mass balance is useful in identifying and optimizing critical parameters in an RW-EDI system [26]. In this study, an empirical mathematical model was formulated and validated using the data obtained from the operation of a single RW-EDI stack in a continuous mode. The model, based on nitrogen balance (Fig. 8a), predicts the number of RW-EDI stacks required for complete NH_4^+ removal. This model is particularly relevant for industrial applications, providing meaningful insights into the scale-up of a RW-EDI system [34]. Simply, the model was formulated with the fractional NH_4^+ removal efficiency of each RW-EDI module (E_N) containing N stacks (Eqn. (12) as presented in Fig. 8b; how the mass of NH_4^+-nitrogen decreased through the treatment process from Steps 1 to 4. The mass of NH_4^+ removal efficiencies of single stacks are approximated by Eqn. (12). The central assumption of the model is that each stack removes a similar mass (mg) of nitrogen from the feed. Therefore, the difference in the mass of NH_4^+-nitrogen between consecutive modules ($m_{N-1} - m_N$) is represented by the constant k, with the material balance derived from experimental data (Fig. 8b).

$$E_1 = \frac{m_0 - m_1}{m_o}, E_2 = \frac{m_1 - m_2}{m_1}, E_3 = \frac{m_2 - m_3}{m_2}, \cdots, E_N = \frac{m_{N-1} - m_N}{m_{N-1}} \quad (12)$$

Substituting $m_{N-1} - m_N$ by k and rearranging the above efficiency equations resulting in Eqn. 13–17. The total efficiency (E_{Total}) of the system with N number of stacks was imperialized to Eqn. (18), which predicts the number of stacks required for a desired efficiency level. For instance, if a single RW-EDI module consistently adsorbs 165 mg of NH_4^+ in a continuous mode, the model estimates that 18 modules are needed to remove 98 % of NH_4^+ from an initial concentration of 3000 mg L^{-1}.

$$E_1 = \frac{k}{m_o} \rightarrow m_o = m_o(1 - E_0) \rightarrow E_1 = \frac{k}{m_o} \quad (13)$$

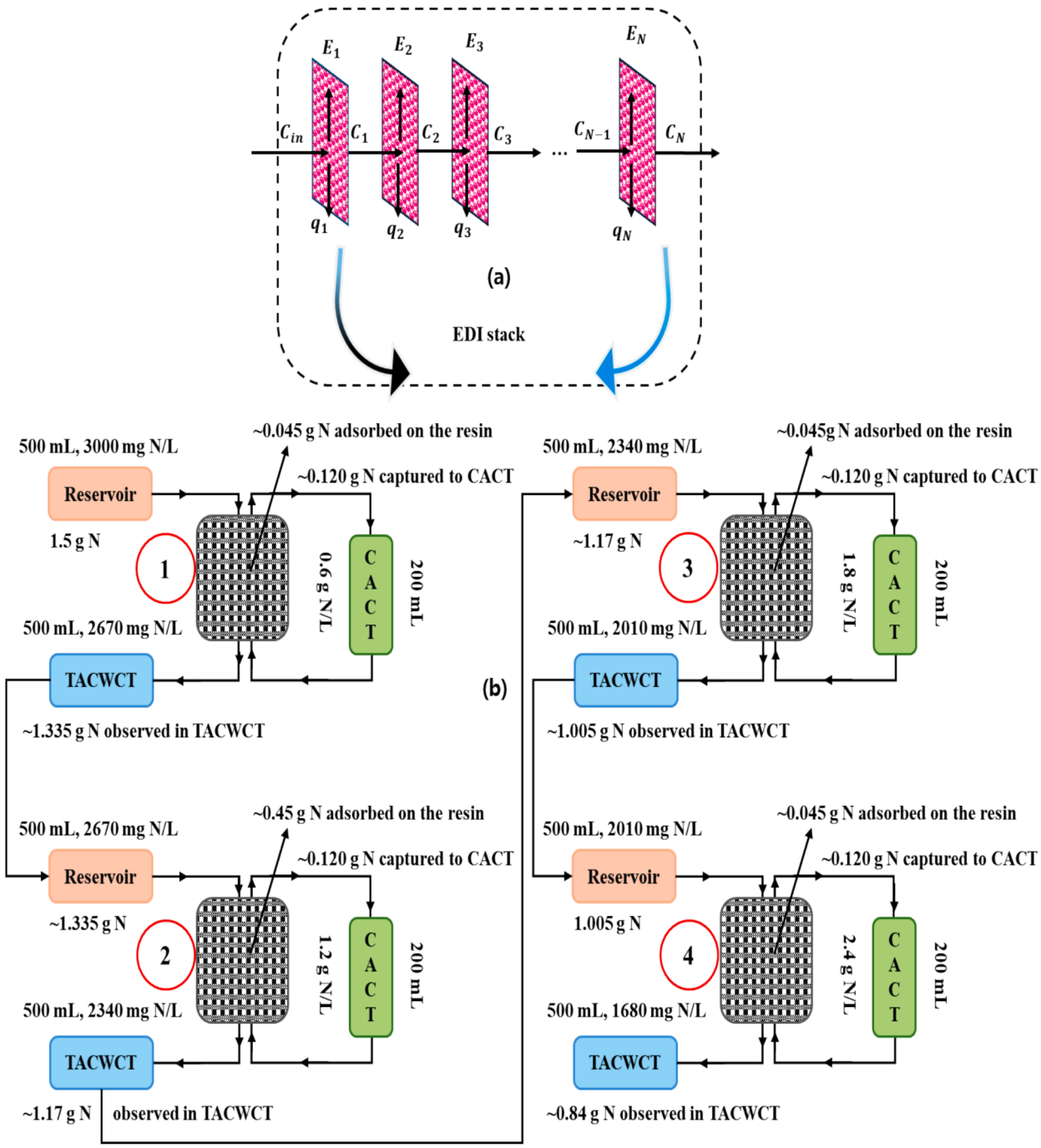

Fig. 8. Simple mass balance model development to determine the number of RW-EDI stacks required to predict for desired NH_4^+ removal (a). Material balance based on nitrogen mass along treatment process (b). The model was developed based on the experimental observation efficiency of a single RW-EDI stack, where E_N is the total efficiency of the RW-EDI, m_o is the initial mass of NH_4^+-nitrogen, m_N is the mass of the NH_4^+-nitrogen at the effluent of N stack, and N is the number of stacks in the RW-EDI system.

$$E_2 = \frac{k}{m_1} \rightarrow m_1 = m_o(1 - E_1) \rightarrow E_2 = \frac{k}{m_o - k} \quad (14)$$

$$E_3 = \frac{k}{m_2} \rightarrow m_2 = m_1(1 - E_2) \rightarrow E_3 = \frac{k}{m_o - 2k} \quad (15)$$

$$E_4 = \frac{k}{m_3} \rightarrow m_3 = m_2(1 - E_3) \rightarrow E_4 = \frac{k}{m_o - 3k} \quad (16)$$

$$E_N = \frac{k}{m_{N-1}} \rightarrow m_{N-1} = m_{N-2}(1 - E_{N-1}) \rightarrow E_N = \frac{k}{m_o - (N-1)k} \quad (170)$$

$$E_{Total}\,(\%) = \frac{Nk}{m_o} \times 100 \quad (18)$$

where E_1 to E_N represent individual efficiencies of the RW-EDI module, m_o is the initial mass of NH_4^+-nitrogen, m_N is the mass of NH_4^+-nitrogen at the effluent of N RW-EDI stack, N represents the number of RW-EDI stacks, k is the resin's adsorption constant, and E_{Total} is the total efficiency.

4. Conclusion

A novel RW-EDI system has been applied for efficient recovering NH_4^+ from wastewater, which consisted of a resin wafer and an ED to offer an energy-efficient alternative to conventional, energy-intensive NH_4^+ removal technologies. In this study, key operating parameters of the RW-EDI such as applied cell voltage, current density, and flow rate were carefully controlled, achieving the NH_4^+ removal efficiency of 80 % over eight cycles. Through the periodic tests and analyses, the point of resin saturation affecting the NH_4^+ removal performance was also determined. When treating water containing 3 g L^{-1} of NH_4^+ at the voltage of 3 V, current density of 2.2 A cm^{-2}, and flow rate of 6.4 mL min^{-1}, the resin wafer became saturated within 90 min, requiring regeneration. When the flow rate and the initial NH_4^+ concentration was adjusted to 2.4 mL min^{-1}, and 1 g L^{-1}, CE and PC were determined to be 41 % and 0.76 kWh m^{-3}, respectively. From the result from the study, it was concluded that the RW-EDI could be a promising alternative to the conventional energy-intensive processes for NH_4^+ oxidation and the nitrogen cycle.

CRediT authorship contribution statement

Redae Nuguse Berhe: Writing – original draft, Visualization, Methodology, Conceptualization, Investigation. **Yu-I Lin:** . **Shu-Yuan Pan:** . **Min Zhan:** . **Hyunook Kim:** Conceptualization, Investigation, Supervision, Writing – review & editing.

Declaration of competing interest

The authors declare that they have no known competing financial interests or personal relationships that could have appeared to influence the work reported in this paper.

Acknowledgment

This work was supported by the green venture research and development program(S3051540) funded by the Ministry of SMEs and Startups (MSS, Korea), and Korea Environment Industry & Technology Institute (KEITI) through the Post Plastic, a specialized program of the Graduate School funded by MOE.

Appendix A. Supplementary data

Supplementary data to this article can be found online at https://doi.org/10.1016/j.cej.2024.157557.

Data availability

Data will be made available on request.

References

[1] A. Zangeneh, S. Sabzalipour, A. Takdatsan, R.J. Yengejeh, M.A. Khafaie, Ammonia removal form municipal wastewater by air stripping process: An experimental study, South African, J Chem. Eng. 36 (2021) 134–141, https://doi.org/10.1016/j.sajce.2021.03.001.
[2] S. Guida, L. Van Peteghem, B. Luqmani, M. Sakarika, A. McLeod, E.J. McAdam, B. Jefferson, K. Rabaey, A. Soares, Ammonia recovery from brines originating from a municipal wastewater ion exchange process and valorization of recovered nitrogen into microbial protein, Chem. Eng. J. 427 (2021) 130896, https://doi.org/10.1016/j.cej.2021.130896.
[3] D. Yang, Q. Chen, R. Liu, L. Song, Y. Zhang, X. Dai, Ammonia recovery from anaerobic digestate: State of the art, challenges and prospects, Bioresour. Technol. 363 (2022) 127957, https://doi.org/10.1016/j.biortech.2022.127957.
[4] S. Kar, R. Singh, P.L. Gurian, A. Hendricks, P. Kohl, S. McKelvey, S. Spatari, Life cycle assessment and techno-economic analysis of nitrogen recovery by ammonia air-stripping from wastewater treatment, Sci. Total Environ. 857 (2023) 159499, https://doi.org/10.1016/j.scitotenv.2022.159499.
[5] Y. hua Li, H. bo Li, X. yang Xu, S. yao Xiao, S. qi Wang, S. cong Xu, Fate of nitrogen in subsurface infiltration system for treating secondary effluent, Water Sci. Eng. 10 (2017) 217–224. https://doi.org/10.1016/j.wse.2017.10.002.
[6] Y. Qin, K. Wang, Z. Zhou, S. Yu, L. Wang, Q. Xia, X. Zhao, C. Zhou, J. Ye, Z. Wu, Nitrogen recovery from wastewater as nitrate by coupling mainstream ammonium separation with side stream cyclic up-concentration and targeted conversion, Chem. Eng. J. 455 (2023) 140337, https://doi.org/10.1016/j.cej.2022.140337.
[7] F. Zhang, X. Li, Z. Wang, H. Jiang, S. Ren, Y. Peng, Simultaneous Ammonium oxidation denitrifying (SAD) in an innovative three-stage process for energy-efficient mature landfill leachate treatment with external sludge reduction, Water Res. 169 (2020) 115156, https://doi.org/10.1016/j.watres.2019.115156.
[8] F. Ulu, M. Kobya, Ammonia removal from wastewater by air stripping and recovery struvite and calcium sulphate precipitations from anesthetic gases manufacturing wastewater, J. Water Process Eng. 38 (2020) 101641, https://doi.org/10.1016/j.jwpe.2020.101641.
[9] J. Nie, H. Huang, P. Rao, H. Chen, X. Du, Z. Wang, W. Zhang, H. Liang, Composite functional particle enhanced gravity driven ceramic membrane bioreactor for simultaneous removal of nitrogen and phosphorus from groundwater, Chem. Eng. J. 452 (2023) 139134, https://doi.org/10.1016/j.cej.2022.139134.
[10] L. He, D. Wang, T. Zhu, Y. Lv, S. Li, Pyrolysis recycling of pig manure biochar adsorption material for decreasing ammonia nitrogen in biogas slurry, Sci. Total Environ. 881 (2023) 163315, https://doi.org/10.1016/j.scitotenv.2023.163315.
[11] T. Elmakki, S. Zavahir, M. Gulied, H. Qiblawey, B. Hammadi, M. Khraisheh, H. K. Shon, H. Park, D.S. Han, Potential application of hybrid reverse electrodialysis (RED)-forward osmosis (FO) system to fertilizer-producing industrial plant for efficient water reuse, Desalination. 550 (2023), https://doi.org/10.1016/j.desal.2023.116374.
[12] S. Dasgupta, A. Atta, Computational insights on intensification of hydrodenitrogenation in a trickle bed reactor using periodic flow modulation, Chem. Eng. Process. - Process Intensif. 157 (2020) 108135, https://doi.org/10.1016/j.cep.2020.108135.
[13] W. Li, X. Shi, S. Zhang, G. Qi, Modelling of ammonia recovery from wastewater by air stripping in rotating packed beds, Sci. Total Environ. 702 (2020) 134971, https://doi.org/10.1016/j.scitotenv.2019.134971.
[14] A.R. Rahmani, N. Navidjouy, M. Rahimnejad, D. Nematollahi, M. Leili, M. R. Samarghandi, S. Alizadeh, Application of the eco-friendly bio-anode for ammonium removal and power generation from wastewater in bio-electrochemical systems, J. Clean. Prod. 243 (2020) 118589, https://doi.org/10.1016/j.jclepro.2019.118589.
[15] P. Ochs, B. Martin, E. Germain-Cripps, T. Stephenson, M. van Loosdrecht, A. Soares, Techno-economic analysis of sidestream ammonia removal technologies: Biological options versus thermal stripping, Environ. Sci. Ecotechnology. 13 (2023) 100220, https://doi.org/10.1016/j.ese.2022.100220.
[16] Y. Tian, S. Wang, L. Pei, K. Zhang, S. Zhu, H. Xu, Z. Ye, Science of the Total Environment Electrochemical mechanism of synchronous ammonia and nitrate removal based on multi-objective optimization by coupling random forest with genetic algorithm, Sci. Total Environ. 901 (2023) 166039, https://doi.org/10.1016/j.scitotenv.2023.166039.
[17] D. Saabas, J. Lee, Recovery of ammonia from simulated membrane contactor effluent using bipolar membrane electrodialysis, J. Memb. Sci. 644 (2022) 120081, https://doi.org/10.1016/j.memsci.2021.120081.
[18] S. Mardani, M. Baghdadi, A. Torabian, B.A. Goharrizi, Journal of Water Process Engineering Optimization of ammonia and COD removal from municipal wastewater effluent by electrochemical continuous flow reactor equipped with Ti / RuO 2 and Cu foam, J. Water Process Eng. 55 (2023) 104185, https://doi.org/10.1016/j.jwpe.2023.104185.
[19] G. Lee, D.Y. Kim, J.I. Han, Gas-diffusion-electrode based direct electro-stripping system for gaseous ammonia recovery from livestock wastewater, Water Res. 196 (2021) 117012, https://doi.org/10.1016/j.watres.2021.117012.
[20] X. Guo, J. Chen, X. Wang, Y. Li, Y. Liu, B. Jiang, Sustainable ammonia recovery from low strength wastewater by the integrated ion exchange and bipolar membrane electrodialysis with membrane contactor system, Sep. Purif. Technol. 305 (2023) 122429, https://doi.org/10.1016/j.seppur.2022.122429.
[21] Z.U. Khan, M. Moronshing, M. Shestakova, A. Al-Othman, M. Sillanpää, Z. Zhan, B. Song, Y. Lei, Electro-deionization (EDI) technology for enhanced water treatment and desalination: A review, Desalination. 548 (2023), https://doi.org/10.1016/j.desal.2022.116254.
[22] S.Y. Pan, S.W. Snyder, H.W. Ma, Y.J. Lin, P.C. Chiang, Energy-efficient resin wafer electrodeionization for impaired water reclamation, J. Clean. Prod. 174 (2018) 1464–1474, https://doi.org/10.1016/j.jclepro.2017.11.068.
[23] T.L. Chen, L.H. Chen, Y.J. Lin, C.P. Yu, H. wen Ma, P.C. Chiang, Advanced ammonia nitrogen removal and recovery technology using electrokinetic and stripping process towards a sustainable nitrogen cycle: A review, J. Clean. Prod. 309 (2021) 127369. https://doi.org/10.1016/j.jclepro.2021.127369.
[24] E.N. Sarıçiçek, M.M. Tuğaç, V.T. Özdemir, İ.Y. İpek, Ö. Arar, Removal of boron by boron selective resin-filled electrodeionization, Environ. Technol. Innov. 23 (2021), https://doi.org/10.1016/j.eti.2021.101742.
[25] K. Khoiruddin, A.N. Hakim, M.A. Alkhadra, M.Z. Bazant, I.G. Wenten, Development and long-term field test of electrodeionization for decentralized desalination facility, Chem. Eng. Process. - Process Intensif. 192 (2023) 109502, https://doi.org/10.1016/j.cep.2023.109502.
[26] F. Qian, J. Lu, D. Gu, G. Li, Y. Liu, P. Rao, S. Fang, N. Zhang, Modeling and optimization of electrodeionization process for the energy-saving of ultrapure water production, J. Clean. Prod. 372 (2022) 133754, https://doi.org/10.1016/j.jclepro.2022.133754.

[27] B.S. Rathi, P.S. Kumar, Continuous electrodeionization on the removal of toxic pollutant from aqueous solution, Chemosphere. 291 (2022) 132808, https://doi.org/10.1016/j.chemosphere.2021.132808.
[28] D. Liao, Y. Pang, Y. Bo, Research on the Ammonia Removal from Synthetic Wastewater by Electrodialysis and Electrodeionization, J. Environ. Eng. 148 (2022), https://doi.org/10.1061/(asce)ee.1943-7870.0002061.
[29] J. Kim, K. Park, D.R. Yang, S. Hong, A comprehensive review of energy consumption of seawater reverse osmosis desalination plants, Appl. Energy. 254 (2019) 113652, https://doi.org/10.1016/j.apenergy.2019.113652.
[30] H. Kalman, D. Portnikov, Analyzing bulk density and void fraction: B, Effect of Moisture Content and Compression Pressure, Powder Technol. 381 (2021) 285–297, https://doi.org/10.1016/j.powtec.2020.12.019.
[31] W. Li, S. Liu, M. Zhang, H. Zhao, P. Zheng, Oxidation of organic electron donor by denitratation : Performance, pathway and key microorganism, Chem. Eng. J. 343 (2018) 554–560, https://doi.org/10.1016/j.cej.2018.02.112.
[32] X.Y. Zheng, S.Y. Pan, P.C. Tseng, H.L. Zheng, P.C. Chiang, Optimization of resin wafer electrodeionization for brackish water desalination, Sep. Purif. Technol. 194 (2018) 346–354, https://doi.org/10.1016/j.seppur.2017.11.061.
[33] A. Fasuyi, A.M. Lopez, Influence of poly(ionic) liquid incorporation within resin wafer electrodeionization for reduced energy consumption in brackish water desalination, Chem. Eng. J. 454 (2023) 140209, https://doi.org/10.1016/j.cej.2022.140209.
[34] C. Otero, A. Urbina, E.P. Rivero, F.A. Rodríguez, Desalination of brackish water by electrodeionization: Experimental study and mathematical modeling, Desalination. 504 (2021) 114803, https://doi.org/10.1016/j.desal.2020.114803.
[35] M. La Cerva, L. Gurreri, M. Tedesco, A. Cipollina, M. Ciofalo, A. Tamburini, G. Micale, Determination of limiting current density and current efficiency in electrodialysis units, Desalination. 445 (2018) 138–148, https://doi.org/10.1016/j.desal.2018.07.028.
[36] H.J. Lee, J.H. Song, S.H. Moon, Comparison of electrodialysis reversal (EDR) and electrodeionization reversal (EDIR) for water softening, Desalination. 314 (2013) 43–449, https://doi.org/10.1016/j.desal.2012.12.028.
[37] R. Zerdoumi, K. Oulmi, S. Benslimane, Electrochemical characterization of the CMX cation exchange membrane in buffered solutions: Effect on concentration polarization and counterions transport properties, Desalination. 340 (2014) 42–48, https://doi.org/10.1016/j.desal.2014.02.014.
[38] S. Park, R. Kwak, Microscale electrodeionization: In situ concentration profiling and flow visualization, Water Res. 170 (2020), https://doi.org/10.1016/j.watres.2019.115310.
[39] P. Sharma, V.K. Shahi, Selective removal of Hg2+/As3+/5+from water system using Suaeda maritima plant based bio-adsorbent hybrid electro-deionization process, J. Environ. Chem. Eng. 10 (2022) 107726, https://doi.org/10.1016/j.jece.2022.107726.
[40] V.V. Nikonenko, A.V. Kovalenko, M.K. Urtenov, N.D. Pismenskaya, J. Han, P. Sistat, G. Pourcelly, Desalination at overlimiting currents: State-of-the-art and perspectives, Desalination. 342 (2014) 85–106, https://doi.org/10.1016/j.desal.2014.01.008.
[41] C. Zhao, L. Zhang, R. Ge, A. Zhang, C. Zhang, X. Chen, Treatment of low-level Cu (II) wastewater and regeneration through a novel capacitive deionization-electrodeionization (CDI-EDI) technology, Chemosphere. 217 (2019) 763–772, https://doi.org/10.1016/j.chemosphere.2018.11.071.
[42] R. Tao, D. Gao, X. Shi, X. Zhu, X. Yang, The relationship between the pH value of dilute effluent streams and system durability in the separate bed electrodeionization process, Sep. Purif. Technol. 247 (2020) 116980, https://doi.org/10.1016/j.seppur.2020.116980.
[43] O.A. Dündar, Ö. Arar, M. Arda, Removal of bromate ions from aqueous solutions via electrodeionization, Environ. Pollut. 339 (2023), https://doi.org/10.1016/j.envpol.2023.122726.
[44] S.O. Abayie, T. Leiviskä, Removal of nitrate from underground mine waters using selective ion exchange resins, J. Environ. Chem. Eng. 10 (2022), https://doi.org/10.1016/j.jece.2022.108642.
[45] Z. Zhang, A. Chen, Simultaneous removal of nitrate and hardness ions from groundwater using electrodeionization, Sep. Purif. Technol. 164 (2016) 107–113, https://doi.org/10.1016/j.seppur.2016.03.033.
[46] F. Sun, G. Wei, H. Du, C. Yang, Performance of continuous electrodeionization technique during the purification of the nonaqueous organic solvent N, N-dimethylformamide, Sep. Purif. Technol. 199 (2018) 242–250, https://doi.org/10.1016/j.seppur.2018.01.063.
[47] D. Liao, Y. Liu, F. Wu, L. Chen, P. Su, D. Feng, Characteristics of nutrient element migration in electrodeionization process, Chem. Eng. Sci. 286 (2024) 119640, https://doi.org/10.1016/j.ces.2023.119640.
[48] R.R. Yaragal, S. Mutnuri, Nitrates removal using ion exchange resin: batch, continuous column and pilot-scale studies, Int. J. Environ. Sci. Technol. 20 (2023) 739–754, https://doi.org/10.1007/s13762-021-03836-8.